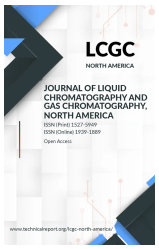

Journal of Liquid Chromatography and Gas Chromatography, North America
https://technicalreport.org/lcgcnam

LC GC N. Am., Vol. 43, No.1, 01-06, 2025

Technical Reports Press

RESEARCH ARTICLE

A Raman-Derived Biophysical Commitment Index for Predicting Nanosecond-Pulsed-Electric-Field-Induced Neuronal Differentiation in PC-12 Cells

Benjamin Scott[1*]

[1]*Institute for Environmental Analysis Greenfield University United States*
[*]*Corresponding author*

Corresponding author:
banjamin_chemist@gmail.com

Received: 21 September 2024
Accepted: 29 December 2024
Available online: 30 March 2025

Abstract

nsPEFsconstitute a temporally sharp physical perturbation, independent of sustained chemical input, for probing the impact on intracellular state. In PC-12 cells, nsPEFs induce neuritogenesis, enhanced neurite outgrowth when NGF-treated, increased C–H Raman scattering intensity, cell volume contraction, and intracellular heating. The research question posed here concerns the existence of a relationship between the early nsPEF-induced changes observable by Raman spectroscopy and the subsequent neuronal commitment of the treated cell population. A novel definition of the Biophysical Commitment Index (BCI), based on cytoplasmic crowding effects, cell-area shrinkage, thermal dynamics of the intracellular medium, and nsPEF-waveform-related parameters, serves as a physiologically motivated predictor of nsPEF-induced neuronal commitment. Herein, the BCI predictor is determined by hierarchical modeling, mediated by Raman-observables and bright-field morphometrics of the individual cells nested within biological replicates, in a way consistent with leave-one-dish-out cross-validation. Contributions of this work include the development of a physically intuitive model relating nsPEF-triggered C–H and O–H vibrations to further neuronal commitment; a validation scheme that accounts for the nested structure of experimental data and preserves the distinction between treatment assignment and early intracellular state; and an experimental design for assessing label-free Raman spectroscopy as a biomarker of drug-free neuronal differentiation.

Keywords: nanosecond pulsed electric fields; Raman microscopy; PC-12 cells; neuronal differentiation; intracellular temperature; molecular crowding; neurite outgrowth; biophysical commitment index

1. Introduction

Neuronal differentiation requires coordinated changes in cell polarity, cytoskeletal organization, membrane trafficking, and transcriptional signaling. These changes underlie neural development and remain central to in vitro models of neural regeneration, disease screening, and cell-based repair strategies [1, 2]. PC-12 cells are widely used for studying neuronal differentiation because they respond reproducibly to nerve growth factor (NGF) by extending neurite-like processes and activating signaling cascades associated with neuronal phenotype acquisition [3, 4, 5]. Their reproducible response makes them a suitable model for evaluating how precisely delivered physical stimulation can influence cell fate.

NGF-based induction has clarified how receptor-mediated signaling regulates neurite outgrowth. NGF activates MAPK and phosphatidylinositol-3-kinase pathways, and the duration of ERK/MAPK activation contributes strongly to the decision between proliferation and differentiation in PC-12 cells [6, 7, 3, 4]. Chemical induction, however, can be difficult to localize, can introduce medium-dependent variability, and often requires prolonged exposure before a morphological endpoint is visible. Physical cues such as electric fields, thermal gradients, mechanical stress, and plasma-generated signals provide complementary routes for controlling cell behavior with high temporal precision [8, 9, 5, 10]. A major barrier to their systematic

Cite as: B. Scott (2025). A Raman-Derived Biophysical Commitment Index for Predicting Nanosecond-Pulsed-Electric-Field-Induced Neuronal Differentiation in PC-12 Cells. LC GC N. Am., 43(1) (2025) 01-06.

This work is licensed under Creative Commons Attribution-NonCommercial 4.0 International License

use is the lack of early, label-free predictors that identify whether a physical stimulus has moved a cell toward a differentiation-permissive state.

Nanosecond pulsed electric fields (nsPEFs) are especially relevant because their short pulse duration and high electric-field strength can perturb intracellular compartments while limiting the irreversible membrane disruption associated with long-pulse electroporation. nsPEFs can form transient nanopores, induce ion flux, alter calcium dynamics, and activate signaling pathways that influence survival, death, and differentiation [11, 12, 13, 14, 15]. In PC-12 cells, 50 ns pulses at approximately 4.5 kV cm^{-1} induce neuronal differentiation without NGF and enhance neurite elongation when NGF is present [16]. In situ Raman microscopy in the same cellular system shows increased C–H stretching intensity, reduction of cell volume to approximately 91%, and an intracellular temperature rise approaching 1 °C during repeated stimulation [16].

These observations raise a mechanistic and practical question: can early Raman-detectable changes predict later neuronal differentiation, or do they only accompany electrical stimulation? A predictive relationship would indicate that nsPEFs generate a definable intracellular state before visible neurite formation. It would also allow Raman microscopy to guide pulse number, waveform, stimulation interval, and NGF co-treatment without waiting several days for neurite outgrowth. The analytical challenge is that C–H intensity, cell shrinkage, O–H-derived temperature change, pulse dose, and NGF status may contribute jointly rather than independently.

This work introduces a Raman-derived Biophysical Commitment Index (BCI) to quantify that joint response. The index tests the hypothesis that nsPEF-induced differentiation is governed by the early intracellular state produced by stimulation, not by pulse exposure alone. The contribution is threefold: Raman and morphometric features are converted into a single interpretable predictor of neuronal commitment; waveform assignment is separated from cell-state information; and validation is performed in a replicate-preserving manner to reduce overfitting and pseudoreplication in nested single-cell data.

2. Biophysical Model

2.1. Physical cell-fate priming

Physical cell-fate priming is defined here as an early intracellular state generated by a non-chemical stimulus that increases the probability of later phenotypic commitment. For nsPEF stimulation, the relevant state may include nanopore-mediated ion transport, calcium mobilization, regulatory volume decrease, cytoplasmic crowding, and transient intracellular thermal cycling [11, 12, 17, 16]. These events can converge on differentiation-associated pathways, including MAPK and phosphoinositide signaling [18, 19].

No single physical readout is expected to be sufficient. Temperature rise, molecular crowding, and cell-volume reduction are treated as complementary components of a multivariable cell state. This choice is supported by the simultaneous changes in C–H intensity, cell area, estimated cell volume, O–H water-band shape, and later neurite outgrowth observed after nsPEF stimulation [16]. A combined index is therefore more informative than a single-marker rule for evaluating whether the early response is consistent with neuronal commitment.

2.2. Definition of the Biophysical Commitment Index

For cell i in dish or biological replicate j, the Biophysical Commitment Index is defined as

$$\begin{aligned} BCI_{ij} = {} & w_1 z(\Delta I_{CH,ij}) + w_2 z(AUC_{T,ij}) + w_3 z(T_{\max,ij}) \\ & + w_4 z(-\Delta A_{ij}) + w_5 z(W_{ij}) - w_6 z(\Delta I_{\mathrm{Amide},ij}), \end{aligned} \tag{1}$$

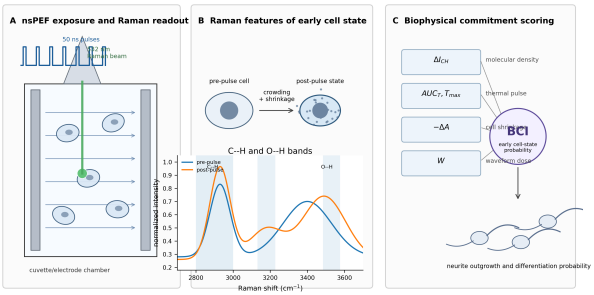

Figure 1: Raman-detectable physical cell-fate priming after nsPEF stimulation. A temporally confined pulse train perturbs PC-12 cells while Raman microscopy captures C–H and O–H spectral responses. Cytoplasmic crowding, transient temperature elevation, and cell-area reduction are integrated into the BCI and evaluated against later neurite outgrowth and differentiation.

where ΔI_{CH} is the normalized change in C–H stretching intensity, AUC_T is the area under the intracellular temperature-response curve, $T_{\max}$ is the maximum intracellular temperature rise, ΔA is the fractional post-stimulation cell-area change, and W encodes waveform-specific exposure. The term $-\Delta I_{\mathrm{Amide}}$ penalizes broad structural disruption because viable nsPEF conditions are not expected to produce strong amide I alterations [16]. The transformation $z(\cdot)$ standardizes each feature within the training data so that all weights operate on comparable scales.

The weights $w_1, \ldots, w_6$ are estimated within the training portion of each validation split by penalized logistic regression, partial least-squares regression, or a Bayesian hierarchical model. Estimating the weights only in training replicates prevents information from the held-out dish from influencing feature scaling or coefficient estimation. A higher BCI indicates stronger early evidence of a differentiation-permissive intracellular state, whereas a lower BCI indicates weak crowding, limited thermal response, minimal area change, or spectral evidence inconsistent with viable priming.

3. Materials and Methods

3.1. Experimental system and measured variables

The analysis is based on the PC-12 nsPEF–Raman measurement record described by Irikura et al. [16]. PC-12 cells were cultured under serum-containing conditions and exposed to pulsed electric fields in cuvette electrodes or under a Raman microscope. The differentiation experiments used a pulse width of 50 ns, voltage of 450 V, repetition frequency of 1 kHz, and total pulse numbers of 30,000 or 90,000 [16]. Neurite assays were conducted with and without 50 ng mL^{-1} NGF. Time-resolved Raman measurements were acquired using a multi-confocal Raman microscope with 532 nm excitation during nsPEF application [16].

The outcome variables are differentiation status, longest neurite length, and neurite-branching morphology. Differentiation is defined by a neurite length exceeding the cell-body diameter, with aggregates of four or more connected cells excluded, consistent with the experimental definition [16]. The early predictors are C–H Raman intensity, O–H water-band temperature ratio, cell-area change, pulse number, waveform category, and NGF status. When cell tracking is available, Raman features and later morphology are linked at the single-cell level. When tracking is unavailable, inference is performed at the replicate level or by distributional matching so that unsupported cell-by-cell pairing is avoided.

3.2. Raman feature extraction

Raman image stacks are processed through a standardized spectral pipeline. Cosmic-ray artifacts are removed, spectra are corrected for baseline drift, and wavenumber calibration is verified before feature extraction. Cellular regions are separated from extracellular background using the clustering-based segmentation strategy applied to the PC-12 Raman measurements [16]. Cellular spectra are normalized against the extracellular water band from 3158 to 3577 cm^{-1} to reduce acquisition-intensity variation.
For each cell, the principal Raman features are

$$I_{CH,ij} = \int_{2800}^{3000} S_{ij}(\nu)\, d\nu, \tag{2}$$

$$R_{OH,ij}(t) = \frac{\int_{3484}^{3576} S_{ij}(\nu,t)\, d\nu}{\int_{3132}^{3228} S_{ij}(\nu,t)\, d\nu}, \tag{3}$$

$$\Delta I_{CH,ij} = I_{CH,ij}^{\text{post}} - I_{CH,ij}^{\text{pre}}, \tag{4}$$

where $S_{ij}(\nu,t)$ is the normalized spectrum of cell i in replicate j at wavenumber ν and time t. The 2800–3000 cm^{-1} C–H band captures changes in intracellular proteins and lipids and is used as a biomolecular-density feature. The O–H ratio is used for temperature estimation because the relative intensities of high- and low-wavenumber water bands vary with temperature-sensitive hydrogen bonding [20, 21, 16].

3.3. Intracellular temperature estimation

Intracellular temperature is estimated from the O–H water-band ratio using the calibration equation

$$R_{OH} = \alpha T + \beta, \tag{5}$$

where R_{OH} is the intensity ratio between the 3576–3484 and 3228–3132 cm^{-1} regions. The PC-12 calibration for this measurement system is highly linear, with a slope close to 0.014 and $R^2 = 0.993$ [16]. Temperature change is therefore calculated as

$$\Delta T_{ij}(t) = \frac{R_{OH,ij}(t) - R_{OH,ij}(0)}{\alpha}. \tag{6}$$

Dynamic thermal features are then defined as

$$T_{\max,ij} = \max_t \Delta T_{ij}(t), \tag{7}$$

$$AUC_{T,ij} = \sum_{t=1}^{m} \Delta T_{ij}(t)\Delta t, \tag{8}$$

$$\rho_{T,ij} = \frac{\Delta T_{ij}(t_{k+1}) - \Delta T_{ij}(t_k)}{t_{k+1} - t_k}, \tag{9}$$

where ρ_T represents local heating or recovery rate. Separating peak temperature rise, cumulative thermal exposure, and recovery kinetics allows the analysis to distinguish a short intracellular thermal pulse from sustained heating.

3.4. Morphological endpoints

Bright-field images are analyzed with a standardized morphometric workflow. Cell-body boundaries are segmented, cell-body diameter is estimated from the equivalent circular diameter or major-axis measurement, and the longest neurite is traced from the cell-body boundary to the distal neurite tip. For each cell, the extracted variables include cell-body area, longest neurite length, number of primary neurites, and number of branch points. Differentiation is coded as

$$D_{ij} = \begin{cases} 1, & \text{if longest neurite length exceeds cell-body diameter,} \\ 0, & \text{otherwise.} \end{cases} \tag{10}$$

The continuous neurite-length endpoint is analyzed in raw units and after $\log(L_{ij}+1)$ transformation to reduce leverage from extremely long neurites. Measurements remain nested within dishes or biological replicates throughout the analysis.

3.5. Statistical modeling

The primary model for differentiation is a hierarchical logistic regression:

$$\begin{aligned}\operatorname{logit}\left[\Pr(D_{ij}=1)\right] =& \beta_0 + \beta_1 BCI_{ij} + \beta_2 N_j + \beta_3 P_j \\ &+ \beta_4 (BCI_{ij} \times N_j) + u_j,\end{aligned} \tag{11}$$

where N_j indicates NGF supplementation, P_j indicates nsPEF exposure, and $u_j \sim \mathcal{N}(0, \sigma_u^2)$ is a dish-level random intercept. The parameter β_1 tests whether the early biophysical state predicts differentiation after adjustment for treatment assignment. The interaction term β_4 tests whether the predictive value of BCI differs when NGF is present. For neurite length L_{ij}, the primary model is

$$\begin{aligned}\log(L_{ij}+1) =& \gamma_0 + \gamma_1 BCI_{ij} + \gamma_2 N_j + \gamma_3 P_j + \gamma_4 (N_j \times P_j) \\ &+ b_j + \varepsilon_{ij},\end{aligned} \tag{12}$$

where b_j is a dish-level random intercept and ε_{ij} is the residual error. A positive γ_1 indicates that the early biophysical state is associated with longer neurites, while a positive γ_4 indicates additional elongation when nsPEF exposure and NGF are combined.

3.6. Mediation analysis

Mediation analysis evaluates whether the association between nsPEF exposure and differentiation is statistically compatible with crowding or thermal response as intermediate variables. For mediator M_{ij}, defined as ΔI_{CH}, $T_{\max}$, AUC_T, or BCI, the system is

$$M_{ij} = a_0 + a_1 P_j + a_2 N_j + u_j + \eta_{ij}, \tag{13}$$

$$\operatorname{logit}\left[\Pr(D_{ij}=1)\right] = c_0 + c' P_j + c_2 N_j + c_3 M_{ij} + v_j. \tag{14}$$

The indirect effect is estimated as $a_1 c_3$ and summarized with bootstrap confidence intervals. This analysis is interpreted as evidence of mechanistic consistency rather than proof of causality because unmeasured variables, including calcium dynamics and osmotic regulation, may also contribute to differentiation.

3.7. Classification and validation

The predictive value of the BCI is evaluated using leave-one-dish-out cross-validation. Each iteration holds out one biological replicate, estimates all preprocessing constants and model weights in the remaining replicates, and evaluates predictions in the held-out replicate. This design avoids optimistic performance estimates caused by sharing cells from the same dish across training and test sets.
Three models are compared:

1. treatment-only model: pulse condition, pulse number, waveform category, and NGF status;
2. Raman-only model: C–H intensity, O–H temperature features, and cell-area change;
3. combined BCI model: treatment variables plus Raman-derived BCI.

Performance is assessed by area under the receiver-operating-characteristic curve, balanced accuracy, calibration slope, calibration intercept, and Brier score. A model is considered experimentally useful only if it improves both discrimination and calibration relative to treatment assignment alone. Permutation testing of outcome labels within dishes verifies that performance exceeds replicate-preserving chance levels.

3.8. Sensitivity analyses

Sensitivity analyses examine whether conclusions depend on threshold definitions, feature selection, or replicate structure. Models are repeated after excluding cells with neurite lengths close to the differentiation threshold. The BCI is recalculated without the temperature terms to test the independent contribution of crowding and cell-area reduction, and then without the C–H term to test the contribution of thermal features. Waveform specificity is evaluated by comparing nanosecond stimulation with microsecond- and millisecond-pulse conditions when those controls are available. Random intercepts are retained in all inferential models to prevent pseudoreplication. Additional robustness checks include bootstrap resampling by dish, assessment of influential replicates, and recalibration of the O–H temperature equation within each measurement session when calibration images are available.

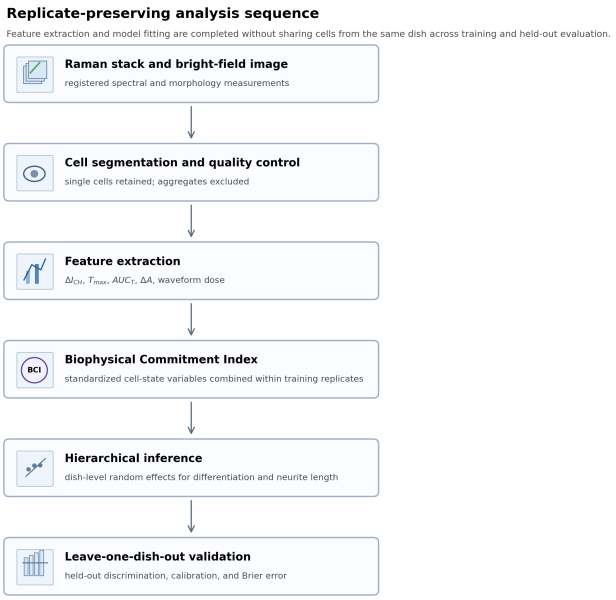

Figure 2: Replicate-preserving analysis workflow linking Raman spectra, bright-field morphometry, BCI construction, mixed-effects modeling, mediation analysis, and leave-one-dish-out validation. Feature extraction and model fitting are completed within the training replicates before prediction in the held-out dish.

4. Results

4.1. Observed responses support a coupled biophysical state

The PC-12 nsPEF–Raman measurement record shows that electrical stimulation produces both morphological and Raman-detectable intracellular changes. The 90,000-pulse condition induced approximately 12% differentiation after six days, while the 30,000-pulse condition produced an intermediate differentiation rate of approximately 8% [16]. No differentiated cells were detected at three days, indicating that nsPEF exposure altered the probability of later phenotype acquisition rather than producing immediate visible neurites.

The same cellular system showed enhanced neurite elongation when nsPEF exposure was combined with NGF, supporting convergence between electrical stimulation and biochemical differentiation cues [16]. Waveform duration was also important: microsecond- and millisecond-pulse conditions did not reproduce the differentiation effect observed with nanosecond pulses. This waveform specificity argues against a nonspecific total-energy explanation and supports the inclusion of a waveform-sensitive exposure term in the BCI.

Raman and morphometric measurements define the early intracellular state captured by the index. nsPEF exposure increased C–H stretching intensity, consistent with increased intracellular biomolecular density. Bright-field measurements showed a reduction of cell area to approximately 94% of the original value and an estimated volume reduction to approximately 91% [16]. The O–H stretching band further indicated transient intracellular temperature increases reaching approximately 0.96 °C during repeated nsPEF application [16]. These coordinated changes justify modeling differentiation as the outcome of a coupled crowding–thermal–morphometric response rather than as a direct function of pulse number alone.

Table 1: Observed nsPEF–Raman responses used to define the Biophysical Commitment Index.

Observation	Biophysical interpretation	Model component
90,000 nsPEF pulses induced approximately 12% differentiation after six days	Pulse exposure shifts the probability of later differentiation	Waveform/exposure term W
30,000 nsPEF pulses produced an intermediate differentiation rate	Differentiation response is compatible with dose-sensitive priming	Dose-sensitive BCI scaling
C–H stretching intensity increased after nsPEF exposure	Intracellular biomolecular density increased	ΔI_{CH}
Cell area decreased to approximately 94%; estimated volume decreased to approximately 91%	Cell shrinkage is consistent with cytoplasmic crowding and regulatory volume change	$-\Delta A$
O–H water-band ratio indicated intracellular temperature rise approaching 1 °C	Stimulation produced transient intracellular thermal pulses	$T_{\max}$ and AUC_T
NGF plus nsPEF enhanced neurite elongation compared with NGF alone	Electrical and biochemical cues converge on neurite outgrowth	$N \times P$ interaction

4.2. Biophysical Commitment Index as an early predictor of differentiation

The BCI converts early Raman and morphometric measurements into a commitment score that can be tested against later cell fate. In the hierarchical logistic model, the principal effect size is the odds ratio for differentiation per one-standard-deviation increase in BCI:

$$\mathrm{OR}_{BCI} = \exp(\beta_1). \tag{15}$$

A value greater than one indicates that cells with stronger early crowding, thermal response, area reduction, and waveform-specific stimulation have higher odds of later differentiation after adjustment for treatment group. This interpretation separates cell-state information from the binary fact of exposure.

The critical validation comparison is not whether nsPEF treatment alone differs from control, but whether Raman-derived state variables improve prediction beyond treatment assignment. The treatment-only model evaluates whether pulse exposure and NGF status are sufficient. The Raman-only model evaluates whether early intracellular features contain independent predictive information. The combined model evaluates whether treatment variables and BCI provide complementary information. Improvement must be demonstrated by cross-validated discrimination and calibration together; an increase in apparent fit without improved held-out calibration is not considered evidence of usable prediction.

4.3. Crowding and thermal response are mechanistically separable

The index is interpretable because its components can be removed or isolated in nested models. If the C–H feature remains positive after adjustment for $T_{\max}$ and AUC_T, biomolecular-density change

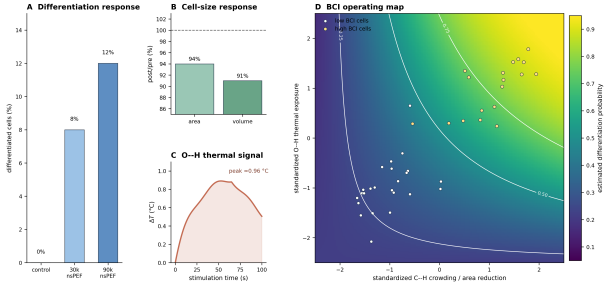

Figure 3: Empirical response summary and BCI operating map for Raman-guided prediction of nsPEF-induced differentiation. The differentiation, cell-size, and thermal panels summarize the numerical response pattern used to motivate the index; the operating map shows how standardized crowding/area and thermal features jointly increase the estimated probability of differentiation during model evaluation.

contributes information beyond temperature. If thermal features remain positive after adjustment for ΔI_{CH} and ΔA, intracellular thermal dynamics contribute information beyond crowding and shrinkage. A combined model with both positive contributions would support a coupled biophysical state rather than a single-mechanism explanation. The nested models are

$$M_0 : D \sim P + N, \tag{16}$$

$$M_1 : D \sim P + N + \Delta I_{CH} + (-\Delta A), \tag{17}$$

$$M_2 : D \sim P + N + T_{\max} + AUC_T, \tag{18}$$

$$M_3 : D \sim P + N + BCI. \tag{19}$$

Model comparison uses likelihood-ratio tests for nested inferential models and cross-validated AUC, Brier score, and calibration slope for predictive models. The combined model is favored only when it improves held-out prediction and retains interpretable positive contributions from the Raman-derived components.

4.4. NGF interaction tests convergence of physical and biochemical cues

Cells receiving both nsPEF exposure and NGF showed greater neurite elongation than cells receiving NGF alone [16]. In Eq. (12), this convergence is represented by γ_4. A positive γ_4 indicates that NGF and nsPEF exposure together produce more neurite elongation than expected from their additive main effects on the log-length scale. If the interaction weakens after inclusion of BCI, the early Raman-defined state partly accounts for the combined effect. If the interaction remains positive after BCI adjustment, NGF and nsPEFs likely contribute through partly distinct mechanisms that converge downstream on neurite elongation. This interaction analysis is essential for biological interpretation because nsPEFs may prime cells through physical changes while NGF activates receptor-mediated signaling. Demonstrating that BCI explains part of the NGF–nsPEF interaction would support a mechanistic link between early intracellular biophysics and later morphological differentiation.

5. Discussion

In this work, we have defined the Raman-based Biophysical Commitment Index as a predictor of nsPEF-induced neuronal differentiation in terms of early intracellular biophysical measurements. The novel aspect of our analysis involves a shift from the conventional treatment group approach to a cell-state approach. The former focuses on whether a specific pulse condition is associated with greater neuronal differentiation than a control treatment. The latter focuses on whether an initial response to a pulse condition can predict subsequent cell fate based on information contained in the response itself.

Biologically, our results have a clear basis because nsPEF stimulation in PC-12 cells triggers a suite of related phenomena that include neuritogenesis in the absence of NGF, enhanced neuritogenesis in the presence of NGF, increased CH content measured via Raman spectroscopy, decreased estimated cellular area and volume, temperature increase inferred from OH vibrations, and waveform selectivity [16]. It is hard to capture these complex changes using a simple physical variable. Hence, the BCI represents neuritogenic potential as a consequence of a complex state of cellular biophysics involving molecular crowding, volume regulation, thermal effects, and electrophysiological perturbation in relation to the stimulation waveforms.

From the perspective of neuronal bioengineering, there is significant practical value in this index because many traditional methods of studying neuronal differentiation are based on measuring the growth of neurites over several days. Raman microspectroscopy is a label-free method that allows acquiring measurements soon after the stimulation, making it suitable for assessing whether a specific pulse protocol created a permissive biophysical environment for neuronal differentiation. Validation in single-cell time course data makes the BCI applicable to the rapid tuning of pulses numbers, fields, frequency, intervals, and NGF co-stimulation conditions.

Statistically speaking, the BCI validation framework takes account of several potential issues associated with single-cell stimulation experiments. All models take into account the correlations between replicate cells derived from the same dish. Feature selection is conducted inside training folds only and, hence, there is no potential bias arising from the use of feature importances across replicate cells in the validation sample. Performance evaluation is based on discriminative power as well as model calibration, which means that even a model with a high discriminatory capacity but poor calibrating abilities would not be overstated. While a high AUC is not sufficient evidence of causality, mediation and removal models test for it separately.

There are some important caveats related to this research. First of all, although PC-12 cells can be used as an approximation of primary neurons, more studies will need to validate the BCI in additional neural models, including neural stem cells. Direct prediction of single cells requires linking measured replicates of Raman-spectra to morphological data obtained from the same cell. In the absence of such a link, it is possible to draw conclusions about prediction only at the level of replicates or distributions. Moreover, the temperature change implied by the O–H band is modest and should be understood in light of the calibration error. Lastly, the BCI is not sufficient for tracing the entire causal chain involved.

All things considered, the BCI offers an important tool for bridging biophysics measured via label-free Raman spectroscopy with nsPEF-induced neuronal differentiation.

6. Conclusion

A Raman-derived Biophysical Commitment Index was developed to connect early intracellular responses with later nsPEF-induced neuronal differentiation in PC-12 cells. The index integrates C–H-based biomolecular-density change, O–H-derived intracellular temperature dynamics, cell-area reduction, and waveform-specific exposure within a hierarchical modeling and replicate-level validation design. By separating treatment assignment from early cell-state information, the analysis provides a rigorous way to test whether Raman-visible biophysical changes predict differentiation and neurite elongation more effectively than exposure labels alone. The approach supports early, label-free optimization of drug-free neuronal differentiation protocols and provides a mechanistically interpretable bridge between bioelectric stimulation and neural phenotype acquisition.

References

[1] Temple, S. (2001). The development of neural stem cells. *Nature, 414*, 112–117.
[2] Yogev, S., & Shen, K. (2017). Establishing neuronal polarity with environmental and intrinsic mechanisms. *Neuron, 96*, 638–650.
[3] Vaudry, D., Stork, P. J. S., Lazarovici, P., & Eiden, L. E. (2002). Signaling pathways for PC12 cell differentiation: Making the right connections. *Science, 296*, 1648–1649.
[4] Santos, S. D. M., Verveer, P. J., & Bastiaens, P. I. H. (2007). Growth factor-induced MAPK network topology shapes Erk response determining PC-12 cell fate. *Nature Cell Biology, 9*, 324–330.
[5] Tominami, K., Kudo, T., Noguchi, T., Hayashi, Y.-R., Luo, T., Tanaka, T., Matsushita, A., Izumi, S., Sato, H., Gengyo-Ando, K., Matsuzawa, A., Hong, G., & Nakai, J. (2024). Physical stimulation methods developed for in vitro neuronal differentiation studies of PC12 cells: A comprehensive review. *International Journal of Molecular Sciences, 25*, 772.
[6] Carter, A. N., & Downes, C. P. (1992). Phosphatidylinositol 3-kinase is activated by nerve growth factor and epidermal growth factor in PC12 cells. *Journal of Biological Chemistry, 267*, 14563–14567.
[7] Marshall, C. J. (1995). Specificity of receptor tyrosine kinase signaling: Transient versus sustained extracellular signal-regulated kinase activation. *Cell, 80*, 179–185.
[8] Ahmed, K., Zaidi, S. F., Rehman, R., Rehman, T., & Kondo, T. (2020). Hyperthermia and protein homeostasis: Cytoprotection and cell death. *Journal of Thermal Biology, 91*, 102615.
[9] Zhang, X., Zhang, S., & Wang, T. (2022). How the mechanical microenvironment of stem cell growth affects their differentiation: A review. *Stem Cell Research & Therapy, 13*, 415.
[10] Kadan-Jamal, K., Wronowski, F., Jin, A., Naegele, T. E., Montes, V. R., Tao, X., Dominguez-Alfaro, A., Lee, C., & Malliaras, G. G. (2025). Electrical stimulation of cells: Drivers, technology, and effects. *Chemical Reviews, 125*, 6874–6905.
[11] Pakhomov, A. G., Bowman, A. M., Ibey, B. L., Andre, F. M., Pakhomova, O. N., & Schoenbach, K. H. (2009). Lipid nanopores can form a stable, ion channel-like conduction pathway in cell membrane. *Biochemical and Biophysical Research Communications, 385*, 181–186.
[12] Semenov, I., Xiao, S., & Pakhomov, A. G. (2013). Primary pathways of intracellular Ca^{2+} mobilization by nanosecond pulsed electric field. *Biochimica et Biophysica Acta–Biomembranes, 1828*, 981–989.
[13] Schoenbach, K. H. (2018). From the basic science of biological effects of ultrashort electrical pulses to medical therapies. *Bioelectromagnetics, 39*, 257–276.
[14] Ruiz-Fernandez, A. R., Campos, L., Gutierrez-Maldonado, S. E., Nunez, G., Villanelo, F., & Perez-Acle, T. (2022). Nanosecond pulsed electric field (nsPEF): Opening the biotechnological Pandora's Box. *International Journal of Molecular Sciences, 23*, 6158.
[15] Joshi, R. P., Garner, A. L., & Sundararajan, R. (2023). Review of developments in bioelectrics as an application of pulsed power technology. *IEEE Transactions on Plasma Science, 51*, 1682–1717.
[16] Irikura, O., Kajimoto, S., Ban, K., & Nakabayashi, T. (2026). Elucidation of neuronal differentiation induced by nanosecond pulsed electric fields using Raman microscopy. *Sensors and Actuators B: Chemical, 463*, 140051.
[17] Yang, Q., Kajimoto, S., Kobayashi, Y., Hiramatsu, H., & Nakabayashi, T. (2021). Regulation of cell volume by nanosecond pulsed electric fields. *Journal of Physical Chemistry B, 125*, 10692–10700.
[18] Morotomi-Yano, K., Akiyama, H., & Yano, K. (2011). Nanosecond pulsed electric fields activate MAPK pathways in human cells. *Archives of Biochemistry and Biophysics, 515*, 99–106.
[19] Tolstykh, G. P., Beier, H. T., Roth, C. C., Thompson, G. L., Payne, J. A., Kuipers, M. A., & Ibey, B. L. (2013). Activation of intracellular phosphoinositide signaling after a single 600 nanosecond electric pulse. *Bioelectrochemistry, 94*, 23–29.
[20] Sugimura, T., Kajimoto, S., & Nakabayashi, T. (2020). Label-free imaging of intracellular temperature by using the O–H stretching Raman band of water. *Angewandte Chemie International Edition, 59*, 7755–7760.
[21] Takahashi, H., Kajimoto, S., Irikura, O., & Nakabayashi, T. (2025). Label-free intracellular temperature measurement by integrating Raman imaging and deep learning. *Chemistry Letters, 54*, upaf032.